Geophys. J. Int. (2007) doi: 10.1111/j.1365-246X.2007.03340.x

Determining the optimal Bouguer density for a gravity data set: implications for the isostatic setting of the Mediterranean Sea

F. Caratori Tontini,[1,2] F. Graziano,[3] L. Cocchi,[1,4] C. Carmisciano[1] and P. Stefanelli[1]

[1] *Istituto Nazionale di Geofisica e Vulcanologia, sede di Portovenere, via Pezzino Basso* 2, 19020, *Fezzano (SP), Italy. E-mail: caratori@ingv.it*
[2] *Consorzio Universitario della Spezia, P.zza Europa* 1, *La Spezia, Italy*
[3] *via Tasso* 36, 24020, *Torre Boldone (BG), Italy*
[4] *Dip.to Sc. Terra Geologiche Ambientali, Univ. Bologna, P.zza Porta S. Donato* 1, *Bologna, Italy*

Accepted 2006 December 23. Received 2006 December 18; in original form 2005 August 17

SUMMARY

We have used free-air gravity satellite data from GEOSAT and ERS-1 missions to compile a Bouguer gravity map of the Mediterranean Sea. The complete Bouguer correction has been applied by using the method of Parker, that acts in the Fourier domain and permits the exact evaluation of the gravity contribution from an highly sampled topographic model of the land. The density used for the Bouguer reduction has been obtained from the gravity data set itself, by using two different optimization methods that have given the same optimal result of 2400 kg m^{-3}. We have studied the radial power spectrum of the data, choosing the optimal Bouguer density from its slope, as the one which minimizes the fractal dimension of the resulting gravity map. The second approach consists of studying the correlation between topography and Bouguer anomaly by spatial cross-plots for a significant subset of the data. Both these approaches are aimed at reducing the short-wavelength effects of topography in the gravity map, but in the past they have been traditionally used alternatively since they gave different optimization values, especially the second method that seems to ignore large-wavelength isostatic effects. Actually, we have revisited both the methodologies, proposing slight modifications to make their efforts compatible. Their coincident results confirm their validity of application and give reliability to the recovered value of the Bouguer optimal density. Moreover, modifying the second approach allows us to compile a sort of normalized correlation map, which we propose in this paper, defining the 2-D isostatic setting of the investigated region without introducing any further lithospheric model. The final result is a revised Bouguer map compiled using a grid with a resolution of 2 min, that is useful for large-scale geological studies and gives important information about the compensation mechanism of the Mediterranean Sea: in a direct way we have found that the overall region seems to be in a complete isostatic equilibrium apart from the young basins of Tyrrhenian Sea and Aegean Sea, confirming previous similar results.

Key words: density, fractals, gravity, isostasy, satellite.

1 INTRODUCTION

Geophysical observations coming from satellite data are of main importance for studying large-scale areas of the Earth surface. Nowadays, however, a Bouguer anomaly map of the Mediterranean Sea from satellite data has not yet been produced, despite of the geological interest of this area. Previous literature concerning the Mediterranean Sea is characterized by the work of Makris *et al.* (1998), compiled by using ship-borne data acquired between 1965 and 1972 by the Osservatorio Geofisico Sperimentale (OGS) of Trieste and on-land data from Department of Geodesy and Geophysics of Cambridge University acquired between 1973 and 1974. This map was produced by using the 1967 normal gravity formula and a standard Bouguer density value of 2670 kg m^{-3}. Considering the significant volume of more recent satellite data we decided to create a revised Bouguer anomaly map, modifying and testing two methodologies aimed at determining the optimal Bouguer density. Bathymetric data come from the database of Naval Oceanographic Office, U.S. Navy, U.S. Dept. of Defence. These data have been gridded at 1-min cell for the Mediterranean Sea, included Black Sea and Adriatic Sea, together with a part of the Atlantic Ocean westward of Gibraltar Straits. The data of Biscay Gulf are instead available at a grid of 2 min (Fig. 1). We used Sandwell & Smith (1997) free-air GEOSAT and ERS-1 combined data sets, which have a grid cell size of 1 min (Fig. 2). Fairhead & Odegard (2002) have shown the effective improvement of satellite gravity data,

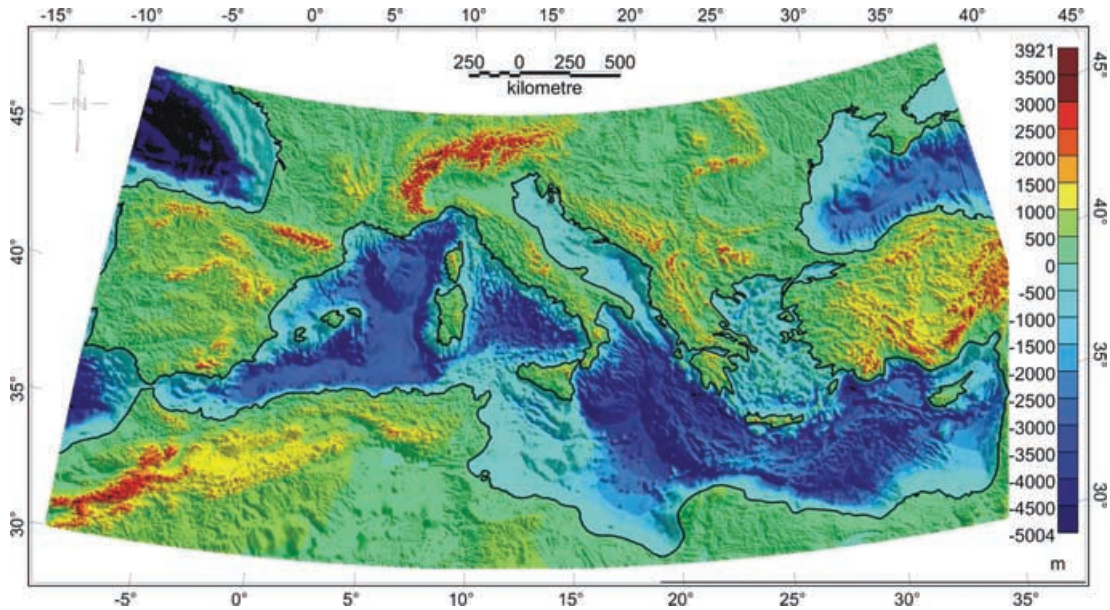

Figure 1. Topographic/bathymetric map of the Mediterranean region.

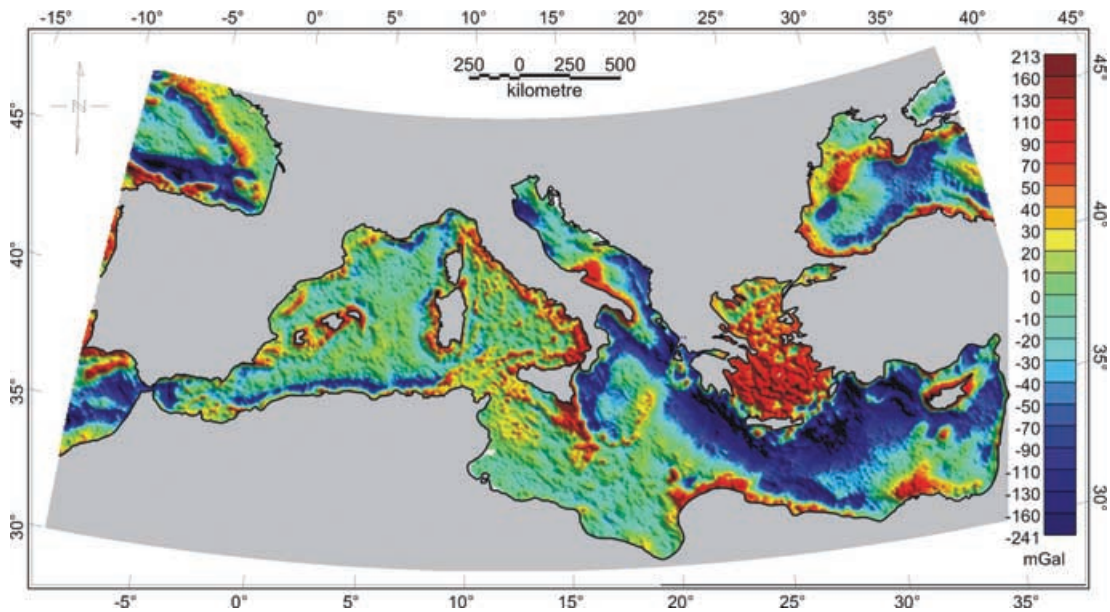

Figure 2. Map of the free-air anomaly of the Mediterranean region estimated by GEOSAT and ERS-1 satellite missions. Land masses are grey-coloured, since gravity anomalies from satellite altimetry are evaluated only on marine areas.

confirming for the high-quality data used in this work the hypothesis of Yale *et al.* (1998) that they are very informative in the range of wavelength $\geq$24 km, that is compatible with the spectral resolution of the bathymetric data. The agreement between gravity anomalies from satellite altimetry and marine data was studied by Andersen & Knudsen (1998), with a particular analysis for the Mediterranean region (Knudsen & Brovelli 1993), where ship gravity data coverage is well represented (Berhend *et al.* 1996). The map of Fig. 1 represents the whole topographic setting of the Mediterranean region, while in Fig. 2 the free-air gravity data are limited to the marine areas since anomalies on land areas can not be estimated from satellite altimetry data. Satellite gravity data on land exist, and are especially devoted to geodetic studies. Recent data from GRACE satellites have reached an accuracy of few millimetres to degree 70 of geoid evaluation (Balmino 2003). However, the spatial resolution of these data is in the range from medium to large wavelength, practically the smallest available wavelengths are in the range 150–300 km. Satellite altimetry provide thus information about anomalies showing wavelengths one order of magnitude smaller, and this is the main reason which dictated the choice of these data, since we are interested into geological–geophysical applications. Since integration of data with different spectral contents is quite difficult, we limit our work to evaluating the Bouguer anomaly map only in the marine areas. The necessary calculation for the Bouguer reduction have been performed by interpolating the gravity and bathymetric data into a common grid with a resolution of 2 min by using

cubic splines. The investigated area extends from 30°N to 48°N and 9.18°W to 37.48°E. The paper proceeds with a section explaining the Bouguer density optimization method that leads to a revised map compiled by the more appropriate value of 2400 kg m^{-3}, significantly different than the standard value of 2670 kg m^{-3}. It is interesting to note that the same reduction density has been used to compile a map of the Bouguer anomaly of Italy and its surrounding seas (Consiglio Nazionale delle Ricerche 1992), based on statistical and rock samples analyses. We expect actually that a reasonable optimization procedure for the ideal Bouguer density value, which is to work on the gravity data themselves, should minimize a meaningful quadratic functional. We will discuss the method used to evaluate the Bouguer correction, and we will analyse in details the choice of the reduction density. Two minimization procedures will be revisited and compared to show their effective agreement after slight modifications aimed at dealing with continental data sets. The global density model so far obtained will be tested by separately analysing the Eastern and Western Mediterranean Basin, and the magnitude of the difference from the Bouguer map compiled with the standard density of 2670 kg m^{-3} will be highlighted. Then we will show some conclusions regarding the isostatic setting of the Mediterranean Sea. We expect thus that this work may be useful for researchers interested in the application of gravity method to the geology of the Mediterranean region, showing also a test for two methodologies that in the past seemed to be quite discordant.

2 DETERMINING THE OPTIMAL BOUGUER DENSITY

The evaluation of the complete Bouguer anomaly for the examined data has been based on the topographic correction alone, since we started from the free-air anomaly (Sandwell & Smith 1997). In order to perform a complete Bouguer correction, it is needed a method able to manage a detailed Digital Elevation Model (DEM) of the land, without splitting the procedure into a simple Bouguer correction by a slab model and then applying the terrain corrections. This is particularly true in a large-scale area as the Mediterranean Sea, both in terms of execution times and automatization of the procedure. Among the vast class of models that exist and allow such calculation, we have chosen the method of Parker (1972) that is particularly suitable for vast areas of the Earth surface because it acts in the Fourier domain, where the greater part of the data processing is usually performed, and it has a very fast convergence provided the vertical origin is chosen at the average topographic level (Parker 1977). Possible limitations deriving from aliasing effects of the 2-D Fourier transformation have been addressed by using a large number of data and by extending the calculation to the area outside of the data extent, also including on-shore topography. Basing on the plane approximation of the 2-D Fourier transform we neglect however curvature effects. The evaluation of the Bouguer correction is mainly expressed in the following equation

$$\Delta G(\mathbf{k}) = 2\pi\gamma e^{|\mathbf{k}|z_0} \sum_{n=0}^{N} \frac{(-|\mathbf{k}|)^{n-1}}{n!} \mathcal{F}\left\{\rho\left[z_t(\mathbf{r})^n - z_b(\mathbf{r})^n\right]\right\}, \qquad (1)$$

where

(i) $\Delta G(\mathbf{k})$ is the anomaly generated by the contrast density $\rho(\mathbf{r})$ in the Fourier domain.

(ii) $\mathbf{k}$ is the wavevector with spatial frequencies k_x, k_y and modulus $|\mathbf{k}| = \sqrt{k_x^2 + k_y^2} = 2\pi/\lambda$.

(iii) z_0 is the data observation level.

(iv) $\gamma = 6.673 \times 10^{-11}$ m^3 kg^{-1} s^{-2} is the Newton gravitational constant.

(v) $z_t(\mathbf{r})$ is the sea level, rescaled with respect to the average depth z_{av} that is chosen as the vertical origin to ensure rapid convergence of the method.

(vi) $z_b(\mathbf{r})$ is the bathymetric level, rescaled with respect to the average depth z_{av}.

(vii) $\mathcal{F}$ indicates the 2-D Fourier operator.

(viii) n is the expansion order coming from the truncation of a Taylor series, our analysis has been stopped for $N = 5$ (N should be ∞ in the theoretical case).

Since we analyse the topographic effect in the marine areas the Bouguer density can be written as:

$$\rho \equiv \rho_W - \rho_B, \qquad (2)$$

where ρ_B is the ideal Bouguer density that is the target of the optimization method and ρ_W is the marine-water density (1030 kg m^{-3}). Practically, we replace the measured topographic effect of water with a slab of thickness given by the bathymetric depth characterized by the same density of the crust. The Bouguer gravity G_B is thus obtained from the free-air anomaly G_{fa} as follows

$$G_B(\mathbf{r}) = \mathcal{F}^{-1}[G_{fa}(\mathbf{k}) - \Delta G(\mathbf{k})], \qquad (3)$$

that is, the Fourier cotransformation of the anomaly to obtain the grid in the spatial domain. These are the basic equations that govern the production of the Bouguer anomaly map. All the input physical quantities depends on the particular topography of the investigated region, apart from the reduction density that is user-dependent. Performing a complete Bouguer reduction involves thus the fundamental task of an appropriate choice of the reduction density ρ_B. The more common value universally accepted is $\rho_B = 2670$ kg m^{-3} that is a reasonable compromise for a certain class of geological models (Hayford & Bowie 1912). As shown by Hinze (2003) this value is 'generally assumed for the density of surface rocks of the continents that are crystalline and of granitic composition'. When possible, different densities from available measurements of the lithologies of the investigated region are used to create an average crustal density down to crust–mantle interface. An approach aimed at the reduction of the topographic contamination of the Bouguer anomaly is probably more effective for continental data sets. Towards this points different methods have been developed by previous authors. Thorarinsson & Magnusson (1990) first and then Chapin (1996) introduced the interesting concept of scaling analysis to reduce the short-wavelength correlation between topography and Bouguer anomaly for a given data set. Their results seemed to be quite discordant concerning the optimization procedure, but we are going to show that probably they are more in agreement than they seem. The concept of minimizing the correlation between topography and Bouguer anomaly however goes far since the pioneering work of Nettleton (1939). The cross-plots of Bouguer anomaly versus topography provide an interesting analysis tool to study this correlation. However, the results obtained by this method seem to ignore the large-wavelength inverse correlation effects typical of isostasy and thus are often used for small regions assumed to be supported by lateral variations in crustal density. However, the very origin of these approaches is the same, that is, reducing the short-wavelength effects of topography in a gravity data set, so that we expect that their result should be consistent at least under slight modifications. In the following subsections, we will revisit both these methodologies showing that under some straightforward assumptions they really match to the same results when applied also to large-scale data sets.

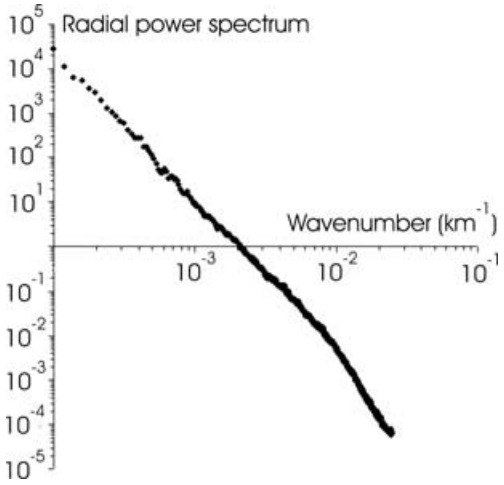

Figure 3. Radial power spectrum of the topography data of Fig. 2. The best-fitting linear trend shows a fractal dimension of 2.77 ± 0.06.

2.1 The scaling approach

The chaotic behaviour of topographic surfaces is well explained in terms of scaling noise (Mandelbrot 1967). The phenomena that lead to the genesis of topography are assumed to be scale-invariant, that is, self-affine at various spatial scales. The scaling behaviour of a particular phenomenon can be checked by analysing its power spectral density by a double-logarithmic scale. It shows, in fact, a linear trend over the various wavelength that translates into a power-law decay with an exponent connected with the fractal dimension of the phenomenon. The dimension D of a scaling surface can be estimated by its radial spectral density, that is, the power spectrum azimuthally averaged over the 2-D wavenumber phase plane by the following equation

$$D = \frac{9+\beta}{2}, \tag{4}$$

where β is the slope, or angular coefficient, of the linear trend that fits the decay of the radial spectrum (Turcotte 1997). Fig. 3 shows the radial spectrum of the topography data of Fig. 1, demonstrating the scaling of these data with a dimension $D = 2.77 \pm 0.06$. Potential-field data can also exhibit a scaling behaviour as demonstrated by previous authors (Gregotski *et al.* 1991; Pilkington & Todoeschuck 1993; Maus & Dimri 1994). The main input when calculating Bouguer anomaly is topography. Its contribution affects the gravity data such strongly that anomalies resemble in many cases the shape of the topography. The connection between Bouguer anomaly and topography is the key to highlight isostasy for the large-wavelength anomalies which are characterized by a negative correlation. The ideal Bouguer density should thus reduce the positive correlation only for the short-wavelength anomalies that are assumed to be supported by lateral variations in crustal density. This approach has been successfully performed in the past by Thorarinsson & Magnusson (1990), who minimized the roughness of the Bouguer anomaly map by varying the reduction density. The roughness derives actually mainly from ragged topography that introduce ragged contour lines also in the gravity map. Their estimation of the fractal dimension was based on a variogram analysis of the gravity anomaly obtaining average densities different than 2670 kg m^{-3} for two regions of Iceland, achieved by minimizing the fractal dimension of the gravity map studied as a 2-D surface, that is, reducing the short-wavelength effect of topography. When there is a large data set as in our case, self-affinity is more rapidly evaluated by the slope of the radial power spectrum by a double logarithmic scale. The work of Chapin (1996) was developed in this sense, by performing a simple Bouguer correction by the slab factor, neglecting terrain corrections, and then by analysing the fractal dimension given by the radial power spectrum in the Fourier domain. His optimization was based on minimization of the difference between a linear decay of the fractal dimension with density and the observed trend. He realized however that his result did not exhibit a minimum for the curve fractal dimension versus density, being thus not compatible with the work of Thorarinsson & Magnusson (1990), that showed instead a U-shaped trend. Chapin (1996) proposed a possible explanation as due to the limited areal extent of Thorarinsson & Magnusson (1990) data to measure accurately the fractal dimension. We think instead that this difference should derive also from the terrain contribution, where the topographic effect play a major role in affecting the short-wavelength gravity field by a scaling contamination. A complete Bouguer correction for the Mediterranean Sea, as obtained by a detailed DEM by the method of Parker (1972) shown in eq. (1), shows the expected parabolic trend with a minimum in agreement with the results of Thorarinsson & Magnusson (1990) as can be seen in Fig. 4(b), where the correct U-shaped curve is well visible. Our minimization has been performed in the range of wavelength from 45 to 105 km where the slope of the radial power spectrum is relatively stable. This band moreover is connected with signals coming

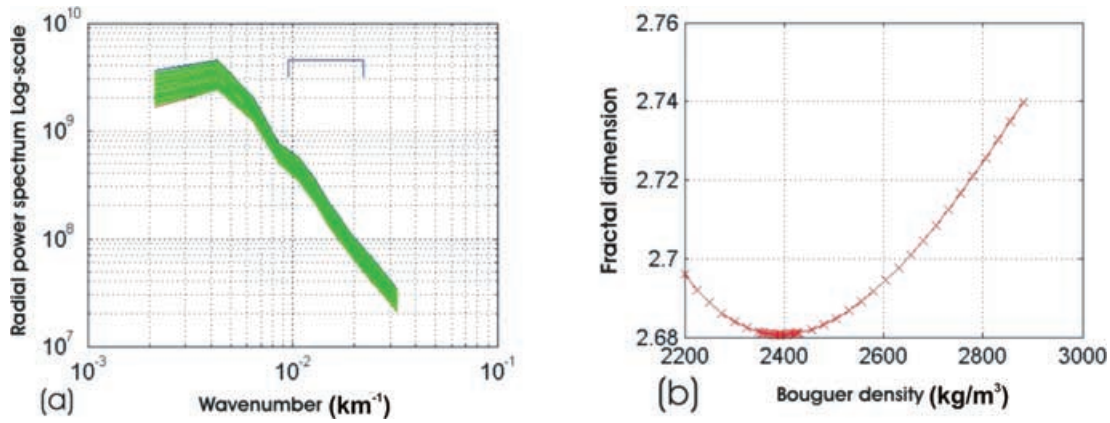

Figure 4. Minimization of the fractal dimension to obtain the optimal Bouguer density. (a) Envelope of the radial power spectra profiles of the Bouguer anomaly for various densities. The blue segment shows the wavenumber band that has been utilized to calculate the fractal exponent that governs the slope of the profiles. (b) Minimization curve of the fractal exponent at varying reduction densities. A least-squares fit has given the optimal density value of 2400 kg m^{-3}.

from intermediate depth sources less influenced by the crust–mantle discontinuity that depends on the particular compensation mechanism. This effect can be seen in the large wavelength part of the radial power spectrum where the slope becomes horizontal indicating non-scaling behaviour as due to isostatic compensation. The fractal dimension shows a minimum value of 2.68 ± 0.07 at $\rho_B = 2400\ \mathrm{kg\,m^{-3}}$ that is the optimal Bouguer density.

2.2 Bathymetry versus Bouguer anomaly cross-plots

The cross-plots of Bouguer anomaly versus topography at varying densities have been widely used to reduce the 'topographic effect' of a given gravity data set. Practically they consists of plotting the Bouguer gravity values versus topography values for each available measurement, to highlight a possible correlation. Ideally this correlation should appear stochastic with a null slope in the case of a perfect rigid crustal support, without isostatic deflection. It is well known instead how isostasy manifests its contribution within a gravity data set, especially in the large-wavelength anomalies that show a negative correlation with topography. This behaviour is particularly evident in Fig. 5, where we have analysed the cross-plots after high-pass filtering, neglecting the wavelength larger than 150 km to reduce the main isostatic correlation effect in the data. We can see that two distinct behaviors are manifested in Fig. 5. The data can be subdivided into two overlapped clouds. We have strongly negative correlated data, supposed thus to be connected with the isostatic compensation mechanism that we label A, together with a subset that shows a quite horizontal slope (subset B). This means that if correlation with topography has to be reduced, it pertains only to the significant subset B of the data. A global minimization of the correlation would produce an underestimation of the optimal Bouguer density, with a consequent flattening of the gravity anomaly also in the case of isostatic large-wavelength features. This is the reason why this approach is usually employed when studying small horizontal extent regions assumed to be supported by lateral variations in crustal density, giving different results with lower optimal Bouguer density with respect to the scaling approach (Thorarinsson & Magnusson 1990). We have tried to solve this problem by performing a simultaneous least-squares fit of the data by using two linear trends, namely line A and line B. Assume a linear relationship for the correlation between Bouguer anomaly and bathymetry

$$y = mx, \tag{5}$$

where y is the Bouguer anomaly, x is the bathymetry and m is the slope of the cross-plots that for ideally uncorrelated data should be null. For a given Bouguer density value the slopes of the lines fitting the overlapping clouds have been determined by varying m as follows

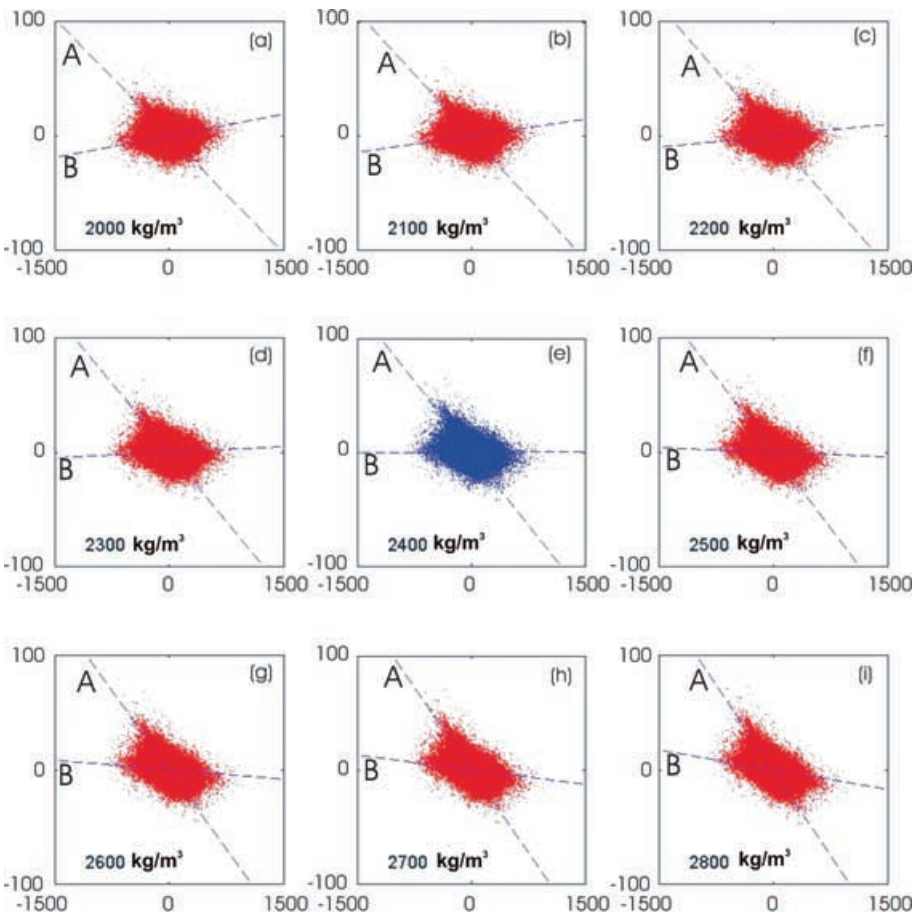

Figure 5. Cross-plots of the correlation between Bouguer anomaly and bathymetry for various reduction densities. Two distinct clouds of points are well isolated in each subplot from (a) to (i). Since the more inclined cloud A is characterized by a strong negative correlation with bathymetry it is believed to be originated by the influence of isostatic compensation in the data. We have found by a double least-squares fit the optimal value of the Bouguer density that makes instead uncorrelated the data of the quasi-horizontal subset B of the data. The optimal value as shown in the central subplot (e) is $2416\ \mathrm{kg\,m^{-3}}$, in good agreement with the value obtained by the scaling analysis of Fig. 4.

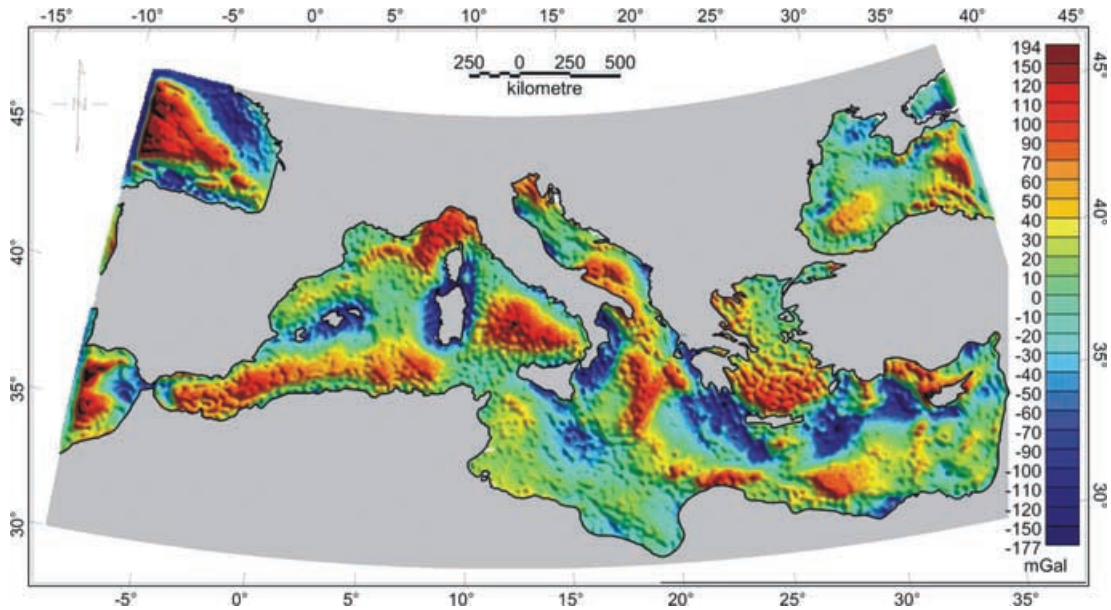

Figure 6. Bouguer anomaly map of the Mediterranean region. The compilation has been done by using a grid with 2 min of resolution, filtering away the small wavelength ≤24 km to be consistent with Yale *et al.* (1998). A0 copies of this map are available by sending a request to the authors of this paper.

(i) $m = m_A$ if the Euclidian distance of the point (x, y) from line A is lower than the distance from line B.

(ii) $m = m_B$ otherwise.

Initial guess for the slopes m_A and m_B must be inputted in the fitting procedure, but at each iteration the values are recalculated in order to converge to the more striking correlation direction between topographic and isostatic pattern. The quasi-horizontal subset B of the data assumes a null slope when the Bouguer density value is 2416 kg m^{-3}, that is in good agreement with the same value obtained by the scaling analysis. Both the methodologies seems thus to give the same optimal results, as we expected due to their same aim of minimizing the short-wavelength 'topographic effect' in the gravity data. Moreover, once we have isolated by the fitting procedure the points that show a strong negative correlation between Bouguer anomaly and topography, namely the group A, we can study their spatial distribution. Since we have assumed that these data may come from relevant isostatic effects, we think that their distribution can give important information about the isostatic setting of the investigated region as we will show in the last section.

2.3 Checking the 2400 kg m^{-3} density model

The map in Fig. 6 shows the Bouguer gravity anomaly that has been compiled using the previously mentioned free-air data set of Sandwell & Smith (1997) and the bathymetric database of U.S. Naval Oceanographic Office, by the revised density of 2400 kg m^{-3}. Besides, the resulting Bouguer anomaly has been low-pass filtered for wavelength lower than 24 km to be consistent with the spectral resolution of Yale *et al.* (1998). It is interesting to see thus, both for a check of the optimization procedure and for the interpretation of its outcome, if a single density model, significantly different from the standard 2670 kg m^{-3}, is appropriate for the huge area of the Mediterranean. To this aim we have subdivided the Mediterranean region into Eastern and Western subregions, separated about 14° longitude, and we have estimated the optimal ρ_B for each subregion. The cross-plots for both the regions are shown in Fig. 7. The optimal densities are 2480 kg m^{-3} for the Western subregion and 2420 kg m^{-3} for the Eastern one. These values are thus in good agreement with the global value of 2416 kg m^{-3} obtained by analysing the whole Mediterranean region, confirming that a global

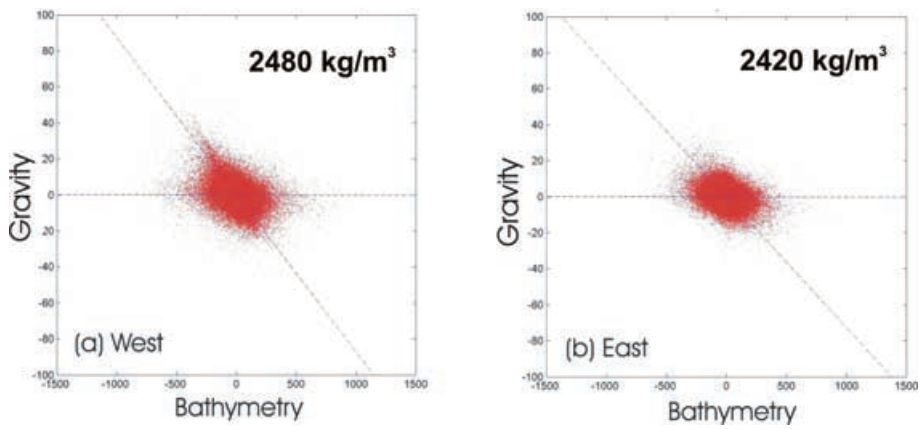

Figure 7. Spatial cross-plots of gravity versus bathymetry for the Western (a) and Eastern (b) subregions. As can be seen the optimal density are close to the global value of 2416 kg m^{-3}.

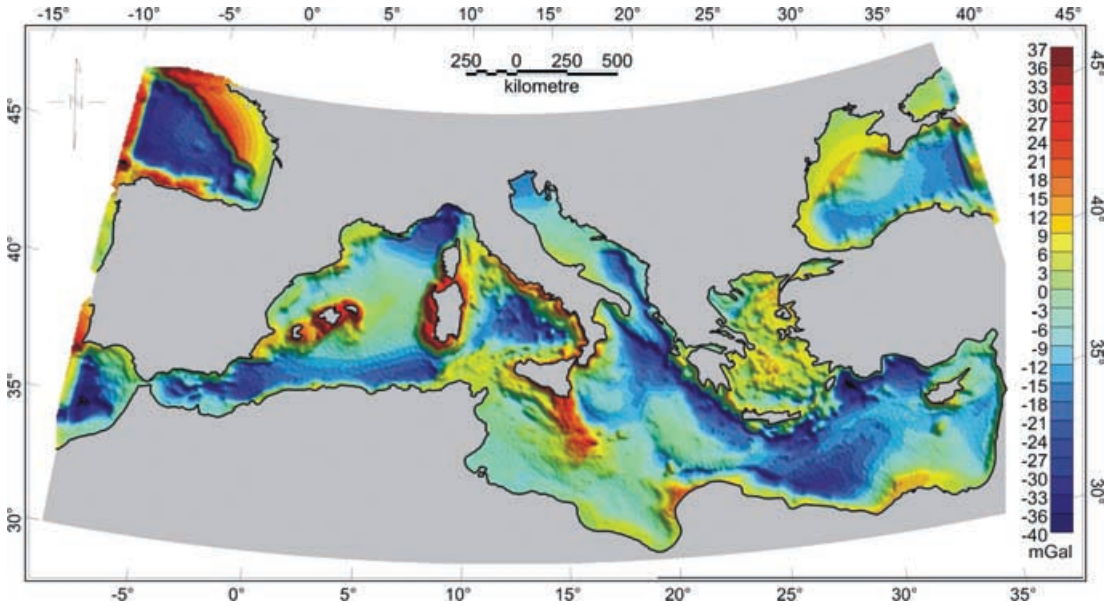

Figure 8. Difference between the Bouguer gravity map compiled with reduction densities 2400 and 2670 kg m^{-3}. The magnitude of this difference do not alter very much the pattern of the Bouguer gravity map of Fig. 6, suggesting thus that the main differences with previous compilation by Makris *et al.* (1998) are due to the new data.

density model with a value lower than the standard 2670 kg m^{-3} may be appropriate all over the Mediterranean region, even taking into account the different tectonic phenomena and the different isostatic regimes that surely characterize this large area. The result implies also a qualitative confirm to the stability of the process of estimating the reduction density as described above. Once we have motivated the choice of the reduction density, we analyse the differences that may appear between our final map (Fig. 6) and the Bouguer map produced with the reduction density previously adopted by Makris *et al.* (1998). This simple map permits us to highlight the differences coming from different values of the reduction density, while it is quite difficult the estimation of the effect deriving from the different origin of the data, that is, satellite altimetry or ship-borne gravity data. Particularly, Fig. 8 shows just the difference between our map compiled with $\rho_B = 2400$ kg m^{-3} and the Bouguer gravity map compiled with $\rho_B = 2670$ kg m^{-3} by using the same altimetry data. Even if the magnitude of the differences can reach 40 mGal, for example within the Tyrrhenian Sea where a deep bathymetry exists, they share the qualitative pattern of the anomalies of Fig. 6 since they are superimposed to intense maxima or minima of the map. This practically means that quantitative differences between similar anomalies may be interpreted as due to the peculiar adopted reduction density. Another striking difference appears in the Aegean Sea, where our map shows a large-scale negative anomaly whose important characteristics will be described in the following section. These differences are important since the Bouguer anomaly is used to constrain forward models of the geological structures, above all in regions as the Mediterranean Sea where, as we will describe in the following section, tectonic processes of backarc spreading and subduction are still in act.

3 DISCUSSION OF THE RESULTS AND CONCLUSIONS

As it stands the map of Fig. 6 can not provide strong information about the isostatic setting of the Mediterranean Sea, even if some important anomalies have been highlighted with respect to previous compilations. Usually additional procedures should be used to highlight the level and depth of compensation (Karner & Watts 1983; Forsyth 1985; McKenzie & Fairhead 1997; Simons *et al.* 2000). Another standard procedure is that of evaluating isostatic residual anomaly to produce a map more suitable for geological exploration (Simpson *et al.* 1986). We believe that these data, after the density optimization, can be usefully employed in order also to produce a map of the isostatic setting of the investigated region, by a straightforward additional processing. When studying the cross-plots between Bouguer anomaly and bathymetry we have identified two subsets of data with different characteristics. By the double fit procedure we have isolated data (group A) supposed to derive from regions where isostasy is evident as demonstrated by the high negative correlation between gravity and bathymetry. The spatial distribution of this subset of data can show some large-wavelength features useful to define the isostatic setting of the Mediterranean Sea. To represent adequately such distribution, we have performed a box-counting method of these points. We have subdivided the region into a set of smaller boxes. Then we have counted the number of points coming from the group A that fall inside of each box. We have normalized this arbitrary number, that we call isostatic level, in the range between 0 and 1 to have a clear 2-D mapping of the isostatic setting. The box size was 20 km and it was chosen as a good balance between the need of a sufficient statistical amount of data inside of each box (which is of order 10^2), and a clear spatial representation of the resulting anomaly as can be obtained by using a large number of boxes. Smaller boxes enclose few data and can not provide useful information, while larger boxes can not show a detailed spatial distribution of the isostatic level. Then we have plotted the spatial distribution of this value as shown in Fig. 9. This procedure may seem a bit unusual, but it is a very fast and simple calculation when the Bouguer density has been evaluated in the way expressed in the previous subsection. We believe that the map obtained by this approach can give some important information. Actually we can see, in fact, that a certain spatial correlation is visible in this map, especially concerning some long-wavelength features that have been

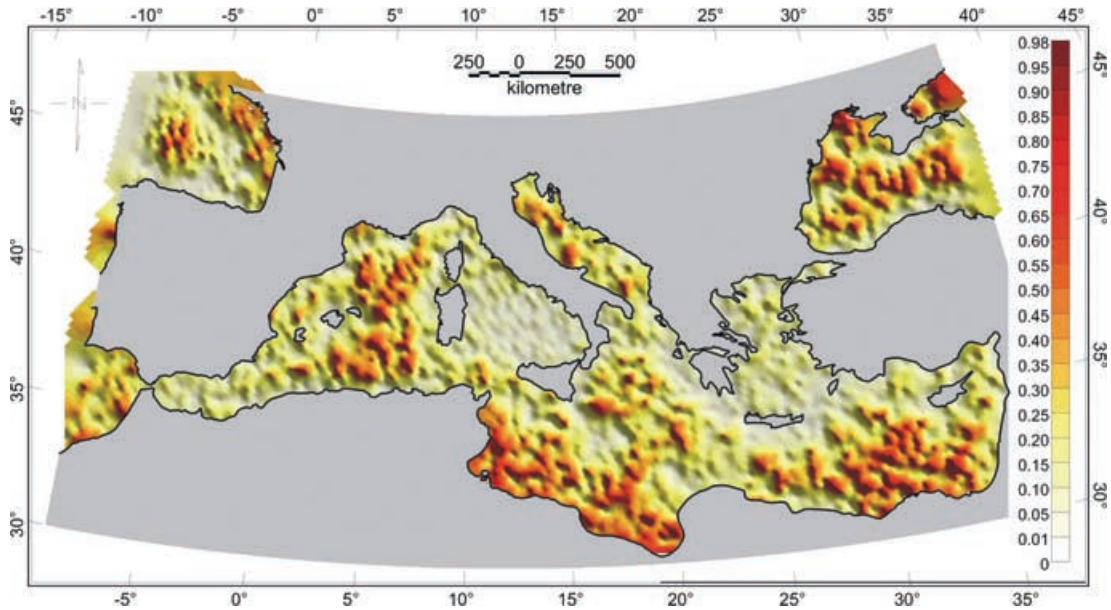

Figure 9. Map of the isostatic setting of the Mediterranean area as obtained by the box-counting method applied to the data where isostatic effect are supposed to play a dominant role. The counting has been rescaled into an arbitrary range between 0 (minimum counting) and 1 (maximum counting). The white areas of the Tyrrhenian Sea and Aegean Sea are well visible, suggesting that these young areas can not be described in the light of a simple isostatic equilibrium.

properly mapped. We would have been more suspicious in front of such a result if it had shown a stochastic behaviour with uncorrelated structures scattered in the investigated region. However, the map seems to show some interesting characteristics, that are in good agreement with results from previous literature. Seber *et al.* (2001), in fact, in a recent paper have investigated the isostatic compensation setting of the Mediterranean Sea. Their analysis is based on a 3-D crustal model obtained by combining sediment thickness, Moho depth, and topography data coming from various observations gridded at 25 km. On the basis of this model they have calculated an Airy-type isostatic anomaly and they have compared their results with the observed gravity to highlight the existence of residuals showing a discordance with the isostatic hypothesis. Our map is in good agreement with their result. The overall Mediterranean Sea, as described by Fig. 9, seems actually to be in nearly complete isostatic equilibrium. High values of the isostatic level are visible all over the map. However, two distinct subregions are characterized by relatively small values of the isostatic level. The first subregion fully characterizes the Southern Tyrrhenian Sea. This region is a relatively young backarc basin characterized by several episodes of of extensional tectonics and volcanism, connected with a SE flexural withdrawal of a subduction system (Malinverno & Ryan 1986; Royden 1988), that suggests a regime of very thin crustal thickness. This hypothesis is confirmed either by maxima values of the heat flow (Della Vedova *et al.* 2001) and by a Moho depth of about 10 km (Sartori *et al.* 2004). Our map of the isostatic level seems to confirm the existence of up-welling mantle at the base of the lithosphere as suggested by Hoernle *et al.* (1995), confirming that the very source of this low isostatic level derive from the upper part of the mantle (Seber *et al.* 2001). The second large-scale anomaly of the isostatic level involves instead the arc characterized by part of Greece offshore, Cyprus and the Aegean Sea since Turkey. Also this region, as the Southern Tyrrhenian Sea, is characterized by a subduction system. Its main direction is NE dipping (Le Pichon & Angelier 1979), with a SW roll-back starting during the Oligocene (Jackson & McKenzie 1988). The 'white' arc of Aegean Sea of Fig. 9 is well known in literature because it represents the distribution of the hypocentres of deep seismicity of this region (Vannucci *et al.* 2004). The presence of these deep seismicity suggests that also this young active region is still undergoing to a compensation mechanism that doesn't reflect a simple isostatic equilibrium of the crust–mantle interface. The anomalies of the isostatic level represented in Fig. 9 seem thus to indicate regions of the Mediterranean Sea characterized by young extensional regimes. In this context the Algero-Provençal Basin, located in the western Mediterranean Sea, between Balearic Sea and Tyrrhenian Sea, seems to behave differently. Actually its genesis is similar to the Tyrrhenian Sea opening, being characterized by an eastward roll-back of extensional tectonics that begun during Oligocene (Carminati *et al.* 1998). However, the genesis of this basin is older with respect to the eastern region of the Mediterranean Sea (30 Ma), and it is tectonically inactive. This could be the reason of this different behaviour, probably motivated by the achievement of the isostatic equilibrium. We have obtained thus a compatible result by determination of a valid criterion for Bouguer density reduction, with a rapid and straightforward procedure, since the optimization seems to provide also information about the isostatic setting of the investigated region. The map of the isostatic level, obtained without introducing any lithospheric model, has highlighted, in fact, two regions of the Mediterranean Sea that were previously identified by Seber *et al.* (2001) as subregions not simply explainable with an Airy-type isostatic compensation mechanism.

ACKNOWLEDGMENTS

We thank the Institutions that have made available the data used for this compilation at the following web-sites:http://www.ngdc.nooa.gov/seg/topo/globe.shtmlhttp://www.mel.navo.navy.mil/data/DBDBV/dbdbv_def.html http://topex.ucsd.edu/WWW_html/mar_grav.html. Prof. J.D. Fairhead is particularly appreciated for his criticisms that improved the earlier version of the manuscript. We thank AE Cynthia Ebinger and two anonymous referees for their competent review.

REFERENCES

Andersen, O.B. & Knudsen, P., 1998. Global marine gravity fields from the ERS-1 and GEOSAT geodetic mission altimetry, *J. geophys. Res.,* **103,** 8129–8137.

Balmino, G., 2003. Gravity field recovery form GRACE: unique aspects of the high precision inter-satellite data and analysis method, *Sp. Sc. rev.* **108,** 47–54.

Berhend, D., Denker, H. & Schmidt, K., 1996. Digital gravity data sets for the Mediterranean Sea derived from available maps, *Bull. d. Inf.,* **78,** 32–41.

Carminati, E., Wortel, M.J.R., Meijer, P.T h. & Sabadini, R., 1998. The two-stage opening of the western-central Mediterranean basins: a forward modeling test to a new evolutionary model, *Earth planet. Sci. Lett.,* **160,** 667–679.

Chapin, D.A., 1996. A deterministic approach toward isostatic gravity residuals—a case study from South America, *Geophysics,* **4,** 1022–1033.

Consiglio Nazionale delle Ricerche, 1992. Structural model of Italy and gravity map, Progetto Finalizzato Geodinamica. *Quaderni de 'La Ricerca Scientifica',* **114**, (9 sheets), CNR.

Della Vedova, B., Bellani, S., Pellis, G. & Squarci, P., 2001. Deep temperatures and surface heat flow distribution, in *Anatomy of an Orogen: The Apennines and Adjacent Mediterranean Basin*, pp. 65–76, eds Vai, G.B. & Martini, I.P., Kluwer Academic, Dordrecht.

Fairhead, J.D. & Odegard, M.E., 2002. Advances in gravity survey resolution, *The Leading Edge,* **21,** 36–37.

Forsyth, D.W., 1985. Subsurface loading and estimates of the flexural rigidity of continental lithosphere, *J. geophys. Res.,* **90,** 12 623–12 632.

Gregotski, M.E., Jensen, O. & Arkani-Hamed, J., 1991. Fractal stochastic modeling of aeromagnetic data, *Geophysics,* **56,** 1706–1715.

Hayford, J.F. & Bowie, W., 1912. The effect of topography and isostatic compensation upon the intensity of gravity, *U.S. Coast Geod. Surv. Spec. Publ.,* **10**.

Hinze, W.J., 2003. Bouguer reduction density, why 2.67?, *Geophysics,* **68,** 1559–1560.

Hoernle, K., Zhang, Y. & Grabham, D., 1995. Seismic and geochemical evidence for large-scale mantle upwelling beneath the eastern Atlantic and Western Europe, *Nature,* **374,** 34–38.

Jackson, J. & McKenzie, D., 1988. Rates of active deformation in the Aegean Sea and surrounding areas, *Basin Res.,* **3,** 121–128.

Karner, G.D. & Watts, A.B., 1983. Gravity anomalies and flexure of the lithosphere at mountain ranges, *J. geophys. Res.,* **88,** 10 449–10 477.

Knudsen, P. & Brovelli, M., 1993. Collinear and cross-over adjustment of Geosat ERM and Seasat altimeter data in the Mediterranean Sea, *Surv. Geophys.* **14,** 449–459.

Le Pichon, X. & Angelier J., 1979. The Hellenic arc and trench system: a key to the neotectonic evolution of the eastern Mediterranean area *Tectonophysics,* **60,** 1–42.

Makris, J., Morelli, C. & Zanolla, C., 1998. The Bouguer gravity map of the Mediterranean Sea (IBCM-G), *Boll. Geof. Teo. Appl.,* **39,** 79–98.

Malinverno, A. & Ryan, W.B.F., 1986. Extension in the Tyrrhenian Sea and shortening in the Apennines as a result of arc migration driven by sinking of lithisphere, *Tectonics,* **5,** 227–245.

Mandelbrot, B.B., 1967. How long is the coast of Britain? Statistical self-similarity and fractional dimensions, *Science* **156,** 636–638.

Maus, S. & Dimri, V.P., 1994. Scaling properties of potential fields due to scaling sources, *Geophys. Res. Lett.,* **21,** 891–894.

McKenzie, D. & Fairhead, J.D., 1976. Estimates of the effective elastic thickness of the continental lithosphere from Bouguer and free air gravity anomalies, *J. geophys. Res.,* **102,** 27 523–27 552.

Nettleton, L.L., 1939. Determination of density for reduction of gravimeter observations, *Geophysics,* **4,** 176–183.

Parker, R.L., 1972. The rapid calculation of potential Anomalies, *Geophys. J. R. astr. Soc.,* **31,** 447–455.

Parker, R.L., 1977. Understanding inverse theory, *Annu. Rev. Earth planet. Sci.,* **5,** 35–64.

Pilkington, M. & Todoeschuck, J.P., 1993. Fractal magnetization of continental crust, *Geophys. Res. Lett.,* **20,** 627–630.

Royden, L., 1988. Flexural Behaviour of the Continental lithosphere in Italy: constraints imposed by gravity and deflection data, *J. geophys. Res.,* **93,** 7747–7766.

Sandwell, D.T. & Smith, W.H.F., 1997. Marine Gravity anomaly from GEOSAT and ERS-1 satellite altimetry, *J. geophys. Res.,* **102,** 10 039–10 054.

Sartori, R., Torelli, L., Zitellini, N., Carrara, G., Magaldi, M. & Mussoni, P., 2004. Crustal features along a W-E Tyrrhenian transect from Sardinia to Campanian margins (Central Mediterranean), *Tectonophysics,* **383,** 171–192.

Seber, D., Sandvol, E., Sandvol, C., Brindisi, C. & Barazangi, M., 2001. Crustal model for the Middle East and North Africa region: implications for the isostatic compensation mechanism, *Geophys. J. Int.,* **147,** 630–638.

Simons, F.J., Zuber, M.T. & Korenaga, J., 2000. Isostatic response of the Australian lithosphere: estimation of the effective elastic thickness and anisotropy using multitaper spectral analysis, *J. geophys. Res.,* **105,** 19 163–19 184.

Simpson, R.W., Jachens, R.C., Blakely, R.J. & Saltus, R.W., 1986. A new isostatic residual gravity map of the conterminous United States with a discussion on the significance of isostatic residual anomalies, *J. geophys. Res.,* **91,** 8348–8372.

Thorarinsson, F. & Magnusson, S.G., 1990. Bouguer density determination by fractal analysis, *Geophysics,* **7,** 932–935.

Turcotte, D.L., 1997. *Fractals and Chaos in Geology and Geophysics*, Cambridge University Press, New York.

Vannucci, G., Pondrelli, S., Argnani, A., Morelli, A., Gasperini, P. & Boschi, E., 2004. An atlas of Mediterranean seismicity, *Ann. Geoph.,* **47** 247–306.

Yale, M., Sandwell, D.T. & Herring, A., 1998. What are the Limitations of Satellite Altimetry?, *The Leading Edge,* **17,** 73–76.